A Computational Study of the Binding of Propidium to the Peripheral Anionic Site of Human Acetylcholinesterase

Andrea Cavalli, Giovanni Bottegoni, Caterina Raco, Marco De Vivo, and Maurizio Recanatini*

Department of Pharmaceutical Sciences, University of Bologna, Via Belmeloro 6, I-40126 Bologna, Italy

Received February 12, 2004

Combined docking and molecular dynamics (MD) simulations were carried out in order to investigate the binding mode of propidium at the human acetylcholinesterase (HuAChE) peripheral site. Two different docking protocols followed by cluster analyses were performed, allowing the identification of five high-populated and low-energy configuration families. To dynamically explore the behavior of the ligand at the peripheral HuAChE binding site, six complexes (five low-energy and one high-energy) were submitted to 2.5 ns of MD simulations. The representative propidium/HuAChE binding modes were chosen on the basis of both the docking energy score and the dynamic stability of the complexes throughout the MD simulations. The most stable poses of propidium at HuAChE PAS were similar to those experimentally determined with the murine enzyme. We therefore suggest that the present modeling protocol might be used in the dynamic investigation of the interactions of a small-molecule inhibitor with a surface-like binding site of a protein. Finally, because of the biological relevance of the target studied here, the present results can be of interest for the rational design of molecules potentially useful in the treatment of the Alzheimer's disease.

Introduction

Noncatalytic actions of enzymes are seldom taken into consideration because the main biological functions of these proteins are linked to the reaction(s) they catalyze. However, articles that recently appeared in the literature show the existence of several examples of important noncatalytic functions for different classes of enzymes.[1−4] Acetylcholinesterase (AChE, EC 3.1.1.7) represents one of the cases where evidence is increasing of a multiplicity of nonclassical roles played by the protein.[5] Here, we show the application of computational methods to the study of structural and dynamic features of the AChE binding site responsible for noncatalytic actions.

AChE is a serine hydrolase that carries out the hydrolysis of the neurotransmitter acetylcholine (ACh), thus terminating its action at the cholinergic synapse. In the past 2 decades, AChE has been the focus of intense research aimed at the discovery of efficient inhibitors in view of their use in treating Alzheimer's disease (AD). These efforts culminated in the development of a number of drugs currently in clinical use.[6] On the other side, the noncatalytic actions of AChE are various and not obvious. They range from cell adhesion to neuritogenesis and synaptogenesis, and from haematopoiesis and thrombopoiesis to promotion of amyloid fibrillization.[5] The latter activity, demonstrated in vitro and in vivo by several teams of researchers,[7−9] is particularly intriguing because it can be related to the neuropathological cascade leading to the AD dementia.[10]

As regards the site on the AChE protein responsible for the noncatalytic actions, studies independently carried out by different laboratories are leading to the conclusion that it coincides or is very close to the so-called peripheral anionic site (PAS) of the enzyme.[11,12] This is a well-known site located at the entrance of the deep catalytic gorge of AChE, and its role in binding substrates and inhibitors has been studied in depth.[13−16] One of the strongest binders at this site is the fluorescence probe propidium (Figure 1), which has been shown to inhibit both the catalytic action of AChE[13] and the AChE-induced fibrillization of amyloid-β (Aβ).[7,8] Other PAS ligands have recently been demonstrated to block the neurite outgrowth stimulatory activity of AChE.[17]

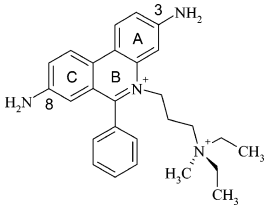

Figure 1. 2D representation of the AChE inhibitor propidium.

The PAS of AChE is composed of amino acid residues identified by X-ray crystallography[18−20] and site-directed mutagenesis[21] experiments. These studies suggested a location of the PAS at the rim of the active site cavity. Actually, in the work of Barak et al.,[21] only a few residues of the array of amino acids involved in the binding of propidium and other PAS ligands could be determined, leading the authors to hypothesize a degeneracy in the composition of the site. A breakthrough in the determination of the PAS composition comes from a recent report on the crystallographic analysis of the interactions between propidium and the mouse AChE (mAChE).[20] These X-ray experiments allowed the identification of the PAS amino acids involved in the interaction with propidium, which was observed to assume two extreme conformations. The disorder in the crystal, due to a range of intermediate positions that a diethylmethylammonium alkyl moiety can assume be-

* To whom the correspondence should be addressed. Phone: 0039 051 2099720. Fax: 0039 051 2099734. E-mail: maurizio.recanatini@unibo.it.

10.1021/jm040787u CCC: $27.50
Published on Web 06/19/2004

tween the extreme ones, makes it difficult to point to a unique binding mode for propidium at the mAChE PAS.[20] This evidence implies the possibility of different binding modes for the PAS ligands and is a reminder of a surface binding situation rather than a typical accommodation into a well-defined binding pocket.

Within the molecular modeling framework, here we use a combined approach of docking and molecular dynamics (MD) simulations to complement the X-ray diffraction experiments and eventually to determine the binding mode(s) of propidium at the PAS of human AChE (HuAChE). By this means, we first screened and energy-ranked different configurations of the ligand/enzyme complex and then simulated the dynamic behavior of six (five low-energy and one high-energy configurations) solvated HuAChE/propidium complexes in a 2.5 ns interval to gain insight on the factors contributing to their formation and stability. The two binding modes of propidium within the PAS, chosen in terms of both low docking energy score and kinetic stability during the MD simulations, turned out to resemble those proposed in the crystal structure of mAChE/propidium complex.[20]

Docking[22] and MD simulations[23] are techniques currently used in most drug design laboratories, and their combined use has recently been applied to the study of the binding specificity of ACh and other ligands to the AChE active site.[24] Such combined approaches might be relevant because, whereas usually enzymes and receptors bind ligands in pockets or cavities located inside the macromolecule, protein−protein interactions such as those probably involved in noncatalytic functions of enzymes occur through external surface sites, which may be univocally determined with difficulty even through X-ray diffraction experiments.

This study represents the first attempt to dynamically investigate the interaction of a small-molecule inhibitor with the peripheral binding site of HuAChE and shows the feasibility of applying molecular modeling to complement a crystallographic study, as already demonstrated in the dynamic study of the conformational plasticity of protein kinases.[25]

Computational Methods

All simulations were based on the crystal structure of the HuAChE refined at 2.76 Å resolution in complex with fasciculin (PDB code: 1B41).[26] Fasciculin was removed from the complex, and the truncated residues Glu268, Gln291, Glu369, and Arg522 were properly completed by means of the Biopolymer module of SYBYL 6.8 (Tripos Inc., St. Louis, MO). Hydrogen atoms were added to the protein amino acids, and the atomic partial charges from the all-atom Amber force field[27] were loaded. Propidium was built by properly adding fragments from the SYBYL standard library to the crystal structure of the 2,7-diamino-9-phenyl-10-ethylphenanthridinium, which was retrieved from the Cambridge Structural Database (CSD code ETHIDB[28]). The three-dimensional model of propidium was geometrically optimized by means of the PM3 semiempirical Hamiltonian[29] as implemented in the SYBYL graphic interface to MOPAC. Atomic partial charges for the propidium molecule were calculated by carrying out single-point ab initio calculations at the HF/6-31G(d) level using the Gaussian 94 package (Gaussian, Inc., Pittsburgh PA, 1994) and then by applying the restrained electrostatic potential (RESP) procedure.[30]

The ligand was docked to the PAS of HuAChE using the DOCK 4.0.1 package.[31] The docking simulations were performed in an "anchor-and-grow" fashion, using the 2,7-diamino-9-phenylphenanthridinium moiety of propidium as anchor part of the molecule. The all-atom Amber force field was used, and the energy estimation was carried out without using the grid approach, to indirectly capture through the point charges the cation−π interaction.[32]

To obtain the widest reasonable coverage of the PAS in the docking procedure, two docking protocols were carried out by considering different definitions of the peripheral binding site. In the first protocol, the PAS was defined as a subset of HuAChE residues within 15 Å from the fasciculin binding site, whereas in the second one, the amino acids within 18 Å from the key residue Trp286 were considered. We reasoned that the difference between the two binding site definitions might reduce the biasing of the PAS exploration by DOCK, still limiting the computational procedure to a reasonably circumscribed protein area. Actually, the binding site based on fasciculin comprised a wider area around the edge of the HuAChE gorge, while the site centered on Trp286 extended more toward the inner portion of the gorge. From each docking protocol, 100 configurations of the propidium/HuAChE complex were ranked according to the DOCK scoring function.[33] To properly group the output docking configurations, geometrical cluster analyses based on an rmsd criterion were performed using an auxiliary program purposely written in Python 2.3. Six representative configurations (five low-energy and one high-energy; see Results) were then submitted to 2.5 ns of MD simulations.

The simulation protocol applied to the propidium/HuAChE complexes was the following: (i) geometry optimization of the hydrogen atoms using the steepest descent (SD) algorithm for 2000 steps; (ii) geometry optimization of the water molecules by means of 2000 steps of SD followed by 3000 steps using the conjugate gradient (CG) algorithm; (iii) energy minimization of the amino acid side chains using SD and CG for 2000 and 3000 steps, respectively; (iv) 20 ps of MD simulations of water box and K^+ counterions at 300 K to equilibrate the solvent; (v) geometry optimization of the whole system (solute plus solvent) by means of 5000 steps of SD and 5000 steps of CG; (vi) 2.5 ns of MD simulations on the whole system.

All the geometry optimizations and MD simulations were carried out using the all-atom Amber force field[27] and the Sander module implemented in the AMBER7 package.[34] The MD trajectories were analyzed by means of the Carnal module of the same package. The internal as well as van der Waals parameters of propidium were determined using an analogy criterion. The ligand/enzyme complexes were immersed in a solvation box of about 13 500 TIP3P water molecules.[35] Six K^+ counterions were added to keep electrostatic neutrality on the whole system. The *NPT* ensemble (constant temperature and pressure) was simulated in periodic boundary conditions by keeping the constant temperature and pressure at 300 K and 1 atm, respectively. Constant temperature and pressure were achieved by coupling the system to a Berendsen's thermostat (time constant for heat bath coupling of 0.5 ps during the equilibration and 1.0 ps during the data collection) and barostat (pressure relaxation time of 0.2 ps).[36] Long-range Coulomb interactions were calculated using the particle mesh Ewald method[37] with ~1 Å charge grid spacing interpolated by fourth-order B-spline and by setting the direct sum tolerance to 10^{-5}. The dielectric constant was set to 1. Short-range Coulomb and van der Waals interactions were estimated within an 8 Å cutoff. The SHAKE algorithm was used to constrain all bonds involving hydrogen atoms.[38] The time step for the integration of the Newton equation was set to 1.5 fs.

Neither constraints nor restraints were applied to the complexes during the MD simulations, allowing the propidium molecule to move freely between the protein surface and the bulk of the solvent.

For all simulations, the rmsd monitored during the MD runs was calculated with respect to the minimized propidium/HuAChE complexes as obtained from the docking studies. For all clusters, the rmsd of propidium non-hydrogen atoms (PRM RMSD) was calculated by superimposing the protein backbone

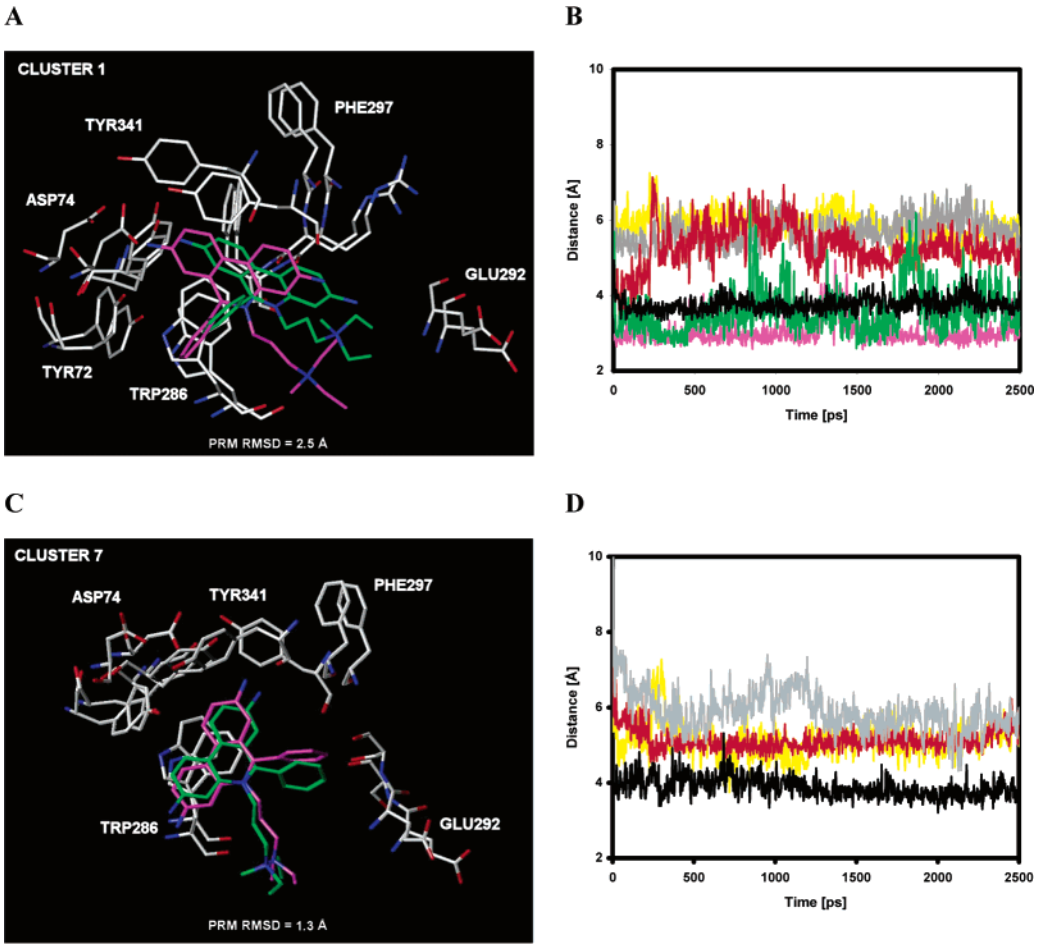

Figure 2. (A) Representative configuration of cluster 1 of propidium within HuAChE PAS (green) and the last conformation (magenta) after 2.5 ns of MD simulations. The rmsd of propidium non-hydrogen atoms (PRM RMSD) is also reported. (B) Distances accounting for the most relevant propidium−PAS interactions during the MD simulations. Phenantridinium moiety center of mass/Trp286 indole ring center of mass is black; propidium N3/carbonyl atom of Ser293 backbone is green; propidium N8/carboxylate group of Asp74 is violet; propidium ring C center of mass/phenolic ring centers of mass of Tyr72, Tyr124, and Tyr341 are yellow, red, and dull-gray, respectively. (C) Representative configuration of cluster 7 of propidium within HuAChE PAS (green) and the last conformation (magenta) after 2.5 ns of MD simulations. The rmsd of propidium non-hydrogen atoms (PRM RMSD) is also reported. (D) Distances accounting for the most relevant propidium−PAS interactions during the MD simulations. Phenantridinium moiety center of mass/Trp286 indole ring center of mass is black; propidium ring A center of mass/phenolic ring centers of mass of Tyr72, Tyr124, and Tyr341 are yellow, red, and dull-gray, respectively.

of the starting conformation onto the protein backbone of the final one (namely, the conformation at 2.5 ns). This allowed us to capture the actual movement of propidium with respect to the PAS residues.

Results

Docking Simulations. From each of the two docking simulations, the first 100 propidium/HuAChE complexes ranked in terms of the energy score were analyzed. Interestingly, the orientations of propidium in the global minimum docking configuration obtained from the two protocols were identical. Cluster analyses of the obtained configurations (200) revealed that they could be grouped into 36 families, showing an intracluster rmsd value less than 3.0 Å for all non-hydrogen atoms. The most populated clusters, which account for 62.5% of all of the orientations, were cluster 1 (48 docking configurations), cluster 2 (17), cluster 4 (23), cluster 5 (20), and cluster 7 (17). Interestingly, in these clusters propidium/HuAChE complexes were ranked with the lowest energy scores. All of the other clusters were both much less populated and characterized by higher docking energy scores such that we assumed configurations representative of clusters 1, 2, 4, 5, and 7 to be worthy of further study. Finally, a representative docking configuration from the quite populated cluster 8 (15 docking configurations), showing an energy score about 7 kcal/mol higher than the global minimum, was selected as a negative control for the subsequent MD simulations (see below).

All of the lowest energy orientations of propidium within the PAS shared a common $\pi-\pi$ stacking interaction between the three-cyclic moiety and the indole ring of Trp286. Actually, in cluster 8, the lack of such an interaction might account for the higher energy score of this binding mode. A second common feature among the lowest energy clusters was the aliphatic chain carrying the quaternary ammonium head, which was never found to point inside the enzyme gorge. Results concerning clusters 1 and 7, which were the most stable ones, are reported in Figure 2, whereas those regarding clusters 2, 4, and 5 are shown in Figure 3. Finally, the results of the outlier cluster 8 are reported in Figure 4.

In the lowest docking energy configuration (cluster 1), propidium established the following interactions with

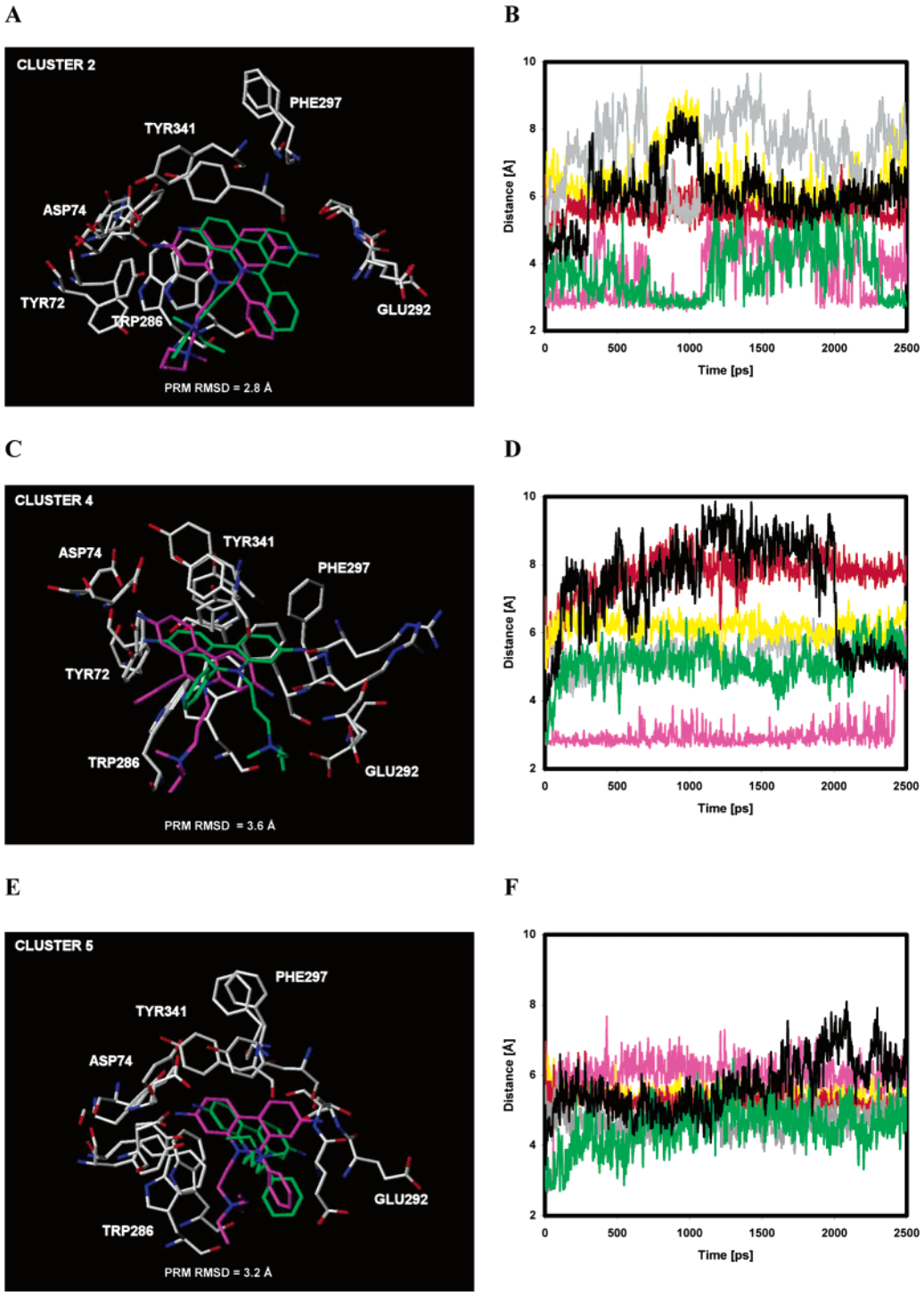

Figure 3. (A) Representative configuration of cluster 2 of propidium within HuAChE PAS (green) and the last conformation (magenta) after 2.5 ns of MD simulations. The rmsd of propidium non-hydrogen atoms (PRM RMSD) is also reported. (B) Distances accounting for the most relevant propidium−PAS interactions during the MD simulations. Phenantridinium moiety center of mass/Trp286 indole ring center of mass is black; propidium N8/carbonyl atom of Ser293 backbone is green; propidium N3/carboxylate group of Asp74 is violet; propidium ring A center of mass/phenolic ring centers of mass of Tyr72, Tyr124, and Tyr341 are yellow, red, and dull-gray, respectively. (C) Representative configuration of cluster 4 of propidium within HuAChE PAS (green) and the last conformation (magenta) after 2.5 ns of MD simulations. The rmsd of propidium non-hydrogen atoms (PRM RMSD) is also reported. (D) Distances accounting for the most relevant propidium−PAS interactions during the MD simulations. The adopted color code is that of Figure 2B. (E) Representative configuration of cluster 5 of propidium within HuAChE PAS (green) and the last conformation (magenta) after 2.5 ns of MD simulations. The rmsd of propidium non-hydrogen atoms (PRM RMSD) is also reported. (F) Distances accounting for the most relevant propidium−PAS interactions during the MD simulations. The adopted color code is that of Figure 3B.

the PAS amino acids (green in Figure 2A): (i) the three-cyclic moiety was in the proper position for a $\pi-\pi$ stacking interaction with the indole ring of Trp286; (ii) the N3 aniline amino group interacted via H-bond with the carbonyl of Ser293 backbone, whereas the other one (N8) bridged the hydroxyl group of Tyr72 and the carboxylate group of Asp74; (iii) the quaternary ammonium head of propidium pointed outward from the

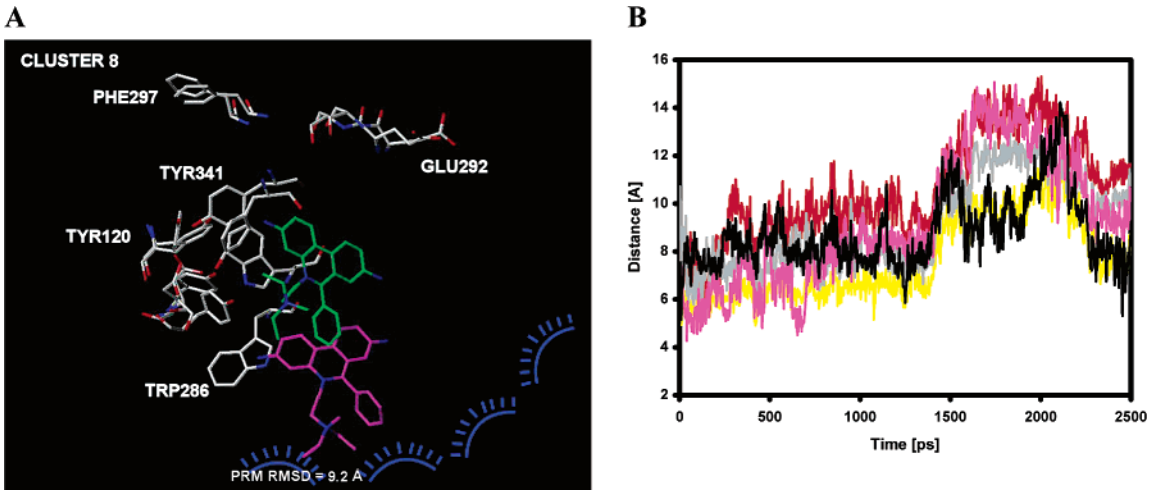

Figure 4. (A) Representative configuration of cluster 8 (outlier) of propidium within HuAChE PAS (green) and the last conformation (magenta) after 2.5 ns of MD simulations. The rmsd of propidium non-hydrogen atoms (PRM RMSD) is also reported. The light-blue lines show the relative position of the bulk of the solvent. (B) Note that the *Y*-axis ranges from 2 to 16 Å. Distances account for the most relevant propidium−PAS interactions during the MD simulations. Phenantridinium moiety center of mass/Trp286 indole ring center of mass is black; propidium N3/carboxylate group of Asp74 is violet; propidium ring A center of mass/phenolic ring centers of mass of Tyr72, Tyr124, and Tyr341 are yellow, red, and dull-gray, respectively.

protein, in the bulk of solvent. Besides the above-mentioned residues, other HuAChE amino acids (namely, Tyr124, Leu289, Arg296, Phe297, and Tyr341) were in proper positions to be involved in hydrophobic interactions with propidium.

In cluster 2 (green in Figure 3A), propidium was flipped about 180° around the phenantridinium symmetry axis with respect to cluster 1. Therefore, the N8 amino group interacted with the Ser293 backbone, while N3 displayed a clear interaction with Asp74. The A-ring fitted into the hydrophobic cage delimited by the aromatic residues Tyr72, Tyr124, and Tyr341. The $\pi-\pi$ stacking between the three-cyclic moiety and the Trp286 indole ring seemed to be less tight than that of cluster 1 because of a narrower interacting surface between the two moieties (Figures 2A and 3A).

Cluster 4 (green in Figure 3C) showed an orientation similar to that of propidium in cluster 1, despite the relevant rmsd (4.26 Å) between the two docking configurations. The main differences were both a sliding movement on the phenathridinium plane, which weakened the $\pi-\pi$ stacking interaction with Trp286, and an increased distance between N8 and the tyrosines-delimited aromatic cage. In addition, the quaternary ammonium head interacted with the carboxylate of Glu292, such an interaction being likely responsible for the good ranking of this cluster.

In the same way, cluster 5 (green in Figure 3E) resembled the orientation proposed in cluster 2 but all of the interactions were less tight, particularly the driving $\pi-\pi$ stacking interaction with the Trp286 indole ring.

The binding mode represented in cluster 7 (green in Figure 2C) was the closest one to the binding mode of propidium in the crystallographic complex with mAChE (PDB code 1N5R).[20] By superimposition of the human and murine enzyme backbones, the rmsd for propidium non-hydrogen atoms was as small as 1.28 Å. The driving interaction was the $\pi-\pi$ stacking with Trp286, whereas N3 interacted with Tyr72, Tyr124, and Tyr337. The most relevant difference with respect to the crystallographic pose of propidium was the lack of an H-bond interaction between one of the amino groups and the Nϵ of the imidazole ring of His287. Likely, this caused cluster 7 to be ranked at a higher docking energy score than cluster 1.

MD Simulations. Because DOCK treats only the ligand in a flexible way, exhaustive protocols of MD simulations were applied, both to relax the propidium/HuAChE complexes and to evaluate the dynamic behavior of the systems at 300 K. This procedure could eventually lead us to assess the feasibility of the binding modes identified by DOCK after taking into consideration further aspects of the ligand/enzyme interaction such as, for example, the induced fit at the binding site and the solvation of the system. To this aim, 2.5 ns of MD simulations sampling the *NPT* ensemble were carried out on the ligand/enzyme complexes representing each of the clusters selected above.

Physicochemical parameters such as temperature, density, potential, and total energy, monitored during the MD simulations, reached stable values for all the complexes after a few hundreds of picoseconds. For all five clusters, both the rmsd of HuAChE backbone and the rmsd of propidium non-hydrogen atoms turned out to be fairly stable throughout the 2.5 ns of MD simulations. More interestingly, some representative interacting distances between propidium and PAS residues were much more stable for clusters 1 and 7. In particular, the driving $\pi-\pi$ stacking interaction between the phenantridinium moiety and the indole ring of Trp286 was by far more stable for clusters 1 and 7 (the black line in parts B and D of Figure 2) with respect to clusters 2, 4, and 5 (the black line in parts B, D, and F of Figure 3) throughout the MD simulations. In the clusters shown in Figure 2, propidium showed a tendency to fluctuate within its binding site, remaining strongly anchored to some PAS amino acids. These results clearly show that clusters 1 and 7 were dynamically more stable during the MD simulations. This was further confirmed by analyzing the rmsd value of propidium non-hydrogen atoms between the starting

and the last MD conformation (magenta in Figures 2A,C and 3A,C,E). Actually, this was as small as 1.3 Å for cluster 7 and 2.5 Å for cluster 1. In cluster 7, which strictly resembled the experimentally determined binding mode of propidium at the mAChE PAS, the rmsd between our model and the crystal structure was slightly reduced after 2.5 ns of MD simulations (1.20 vs 1.28 Å for all of the propidium non-hydrogen atoms). More interestingly, the MD simulations were able to account for the induced-fit effects, allowing the ligand to properly be accommodated at the HuAChE PAS. Actually, despite the low rmsd between the orientation of propidium in cluster 7 and the experimental one, MD simulations carried out on a system simply built by merging propidium from the crystallographic complex to the HuAChE PAS did not provide reliable dynamic results (data not shown). In such a simulation, propidium turned out to be highly unstable, leaving the HuAChE PAS already after a few hundreds of picoseconds likely because ligand and target could not properly fit each other.

Clearly, the clusters shown in Figure 3 turned out to be less stable than both clusters 1 and 7. Actually, although cluster 2 also showed a low rmsd value (2.8 Å; see Figure 3A) between the starting and the last MD conformations, the most important interactions with PAS residues were fairly unstable throughout the 2.5 ns of MD simulations, as reported in Figure 3B. Cluster 4 coupled an rmsd value of 3.6 Å (Figure 3C) to a clear instability of the monitored interactions (Figure 3D). Cluster 5, showed an rmsd value of 3.2 Å (Figure 3E) and a clear instability of both the driving $\pi-\pi$ stacking with Trp286 and the interaction between propidium atom N8 and the carbonyl oxygen of the Ser293 backbone (Figure 3F). Clusters 2, 4, and 5 binding modes could be considered representative of intermediate orientations, where key interactions were not strong enough to be preserved throughout the MD simulations.

In contrast, the pose representative of a quite populated but high-energy-ranked cluster (cluster 8, Figure 4) showed remarkably different behavior. In cluster 8, propidium left the binding site moving toward the bulk of the solvent. All of the most important interactions with the HuAChE PAS residues were lost after 1.4 ns of MD simulations (Figure 4B). The final rmsd value of propidium non-hydrogen atoms between the starting and the last MD conformation was equal to 9.2 Å (Figure 4A). Because this cluster was the lowest one among those at higher energy, we assumed that none of the other higher energy clusters would have been able to converge to a stable binding mode.

Discussion

The crystal structure of mAChE in complex with propidium appeared recently in the literature.[20] Although the authors state that mAChE PAS can accommodate propidium with two distinct conformations related by a 180° flip around the phenantridinium symmetry axis, only one complex is reported in the PDB file (PDB code 1N5R). Therefore, in this study, we tried to identify some other possible orientations of propidium within the PAS of HuAChE by means of docking and MD simulations. The high similarity between mAChE and HuAChE sequences (sequence identity equal to 88%) makes it possible to compare the present results to those experimentally obtained with the murine enzyme. The choice of propidium binding modes at HuAChE PAS was done considering both the docking energy score and the dynamic stability of the complexes throughout the 2.5 ns of MD simulations, thus implying that only the combination of the two computational techniques may provide reasonable results. Actually, taking into account only the docking energy score, cluster 7, which strictly resembles the crystallographic propidium binding mode at the mAChE PAS, would not have been selected. Similarly, MD alone could not have been able to provide an adequate description of the ligand/protein complex because a reliable starting configuration is required for this aim. This clearly illustrates the need to use a combined approach both to provide a reliable starting ligand/target complex and to allow the protein and the ligand to properly fit each other and eventually stabilize the binary molecular complex.

This computational protocol might be usefully applied to the study of the binding of ligands to surface sites of proteins, such as those involved in protein−protein interactions. X-ray crystallography sometimes might partially fail in resolving univocally the structures of complexes between proteins and small-molecule ligands bound to the surface of a macromolecule. This might be possibly due to the inherent difficulty of growing crystals of such loose complexes or of soaking low-affinity ligands. Here, we showed that by application of a proper computational protocol, it is possible to develop interaction models of this kind of complex with the aim of complementing X-ray diffraction experiments to be eventually challenged by kinetic or mutagenesis studies.

Binding of Propidium to the PAS. The present findings point to two possible configurations (parts A and B of Figure 5) as the limits of a range of intermediate positions available for the binding mode of propidium within the HuAChE PAS, as previously detected in the crystallographic complex between mAChE and propidium.[20] As regards the binding interactions, the $\pi-\pi$ stacking between the phenantridinium moiety and the indole ring of Trp286 was shown to be the driving force for the binding, as was always observed for all of the lowest energy docking configurations. Furthermore, considering that this $\pi-\pi$ interaction seemingly allows the aromatic rings to slide rather freely from one to the other (a true "pivotal" role), it is not surprising that there are a number of different configurations of the propidium/HuAChE complex here determined.

One of the two binding modes (Figure 5B) was strikingly similar to the configuration determined for mAChE/propidium crystallographic complex and reported in the PDB (rmsd = 1.20 Å, after 2.5 ns of MD simulations). The second binding mode here identified (Figure 5A), which represented both the global minimum configuration and the most populated cluster, resembles the second binding mode suggested by the authors for the mAChE/propidium crystallographic complex.[20] However, a direct comparison in terms of rmsd was not possible because a simple flip of 180° around the phenantridinium axis of the crystallographic propidium/mAChE complex did not lead to a reasonable binding mode because of relevant clashes between the

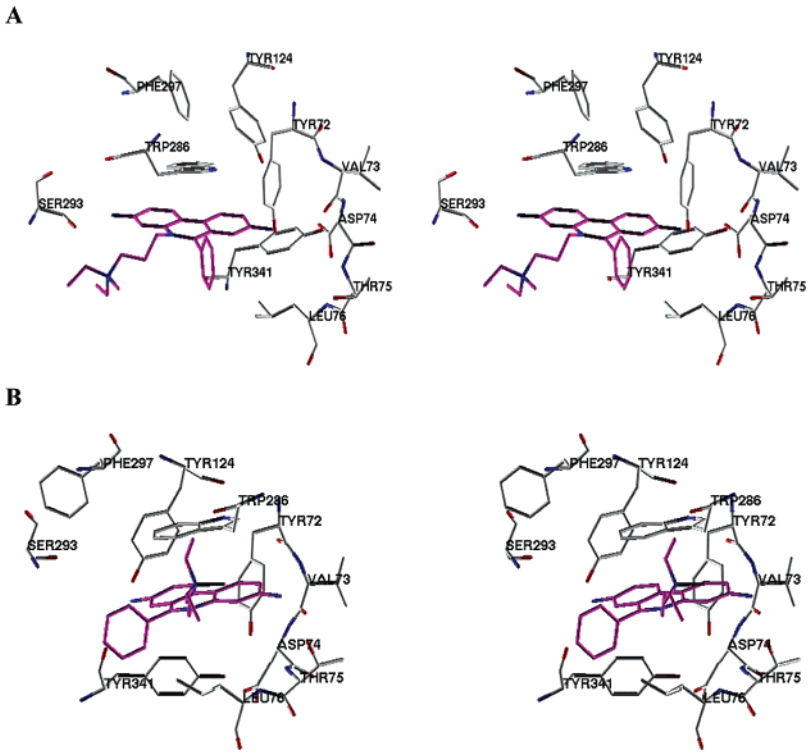

Figure 5. (A) Stereoview of a minimized snapshot at 2.5 ns from the MD simulations of cluster 1. Carbon atoms of propidium are magenta. (B) Stereoview of a minimized snapshot at 2.5 ns from the MD simulations of cluster 7. Carbon atoms of propidium are magenta.

ligand and some PAS amino acids. The other intermediate configurations turned out to be much less stable throughout the MD simulations, likely as a consequence of their lower thermodynamic and/or kinetic stability. We might speculate that longer protocol of MD simulations (likely in the range of tens ns) could allow clusters 2 and 5 to converge to cluster 7, and cluster 4 to cluster 1.

The two binding modes of the propidium depicted in Figure 5 can be discussed in light of previous experimental and theoretical findings. The main characteristic of these models is the interaction between the phenantridinium moiety of propidium and the indole ring of Trp286, in good agreement with the X-ray structure[20] and mutagenesis experiments.[21] Actually, it seems that only interactions such as $\pi-\pi$ stacking might be able to catch propidium from the aqueous environment where H-bonds and electrostatic interactions can be stronger than those between propidium and the PAS residues. This observation is consistent with the results obtained from the MD simulations carried out on cluster 8 (Figure 4). In this cluster, the $\pi-\pi$ stacking between the indole ring and the phenantridinium moiety was not identified and the ligand left the PAS after some hundreds of picoseconds. In this regard, it should be remembered that in the propidium/HuAChE systems here studied, the ligand was allowed to move freely looking for its best position of binding at the PAS and that the PAS, located at the mouth of the deep active site cavity, is very exposed to the solvent. Indeed, we considered the systems to be wholly solvated, and a consequence thereof might have been that a hydrophilic molecule like propidium (estimated[39] $\log P = -4.3$) tended to escape the binding site, looking for a more convenient environment in water. Actually, cluster 8 clearly showed the tendency of propidium to move toward the aqueous environment (Figure 4), probably just because of the lack of the $\pi-\pi$ stacking between the indole of Trp286 and the phenantridinium. In light of these results, it is hypothesized that protein surface binding sites should be composed of aromatic and/or hydrophobic residues rather than polar or charged amino acids because water molecules from the bulk of the solvent can strongly compete with the interactions that residues of the latter kind can establish with ligands.

Besides the fundamental role of Trp286, our proposed models point to a subset of aromatic residues around Trp286 responsible for the binding of propidium to the HuAChE PAS, in agreement with the above-mentioned mutagenesis experiments.[21] In particular, the two tyrosines Tyr72 and Tyr341 together with a third one (Tyr124) constitute a small aromatic cage able to host rings C or A of the phenantridinium moiety. In contrast, in the crystal, besides the $\pi-\pi$ stacking between Trp286 and propidium, the only other direct interaction between enzyme and ligand was an H-bond connecting one of the amino groups and Nϵ of the imidazole ring of His287.[20] Interestingly, by superimposition of the backbone of murine and human AChE crystal structures (PDB codes 1N5R and 1B41, respectively), it is possible to see a perfect superimposition of the Trp286 residues (rmsd = 0.57 Å), whereas the two His287 show an rmsd of 1.3 Å. Also, the distance between the Nϵ of the two histidines is as high as 2.3 Å, thus not allowing His287 of HuAChE to interact with propidium by means of the H-bond disclosed by the X-ray experiments carried out with mAChE. This probably caused cluster 7 (closest to the crystallographic pose) to be energetically less stable than cluster 1 where the ligand was able to

interact with Trp286 and with Ser293 and Tyr124 through H-bonds. After 2.5 ns of MD simulations, the rmsd between the mAChE and HuAChE histidines increased to 4.4 Å, making it even more unlikely for the interaction to be captured. In light of these results, we might infer that even longer MD simulations would not have allowed us to identify the interaction between propidium and His287 mainly because of the high dynamic stability of cluster 7.

While our results are in line with the hypothesis of propidium binding at the peripheral site, a remarkable but hardly rationalizable increase of resistance to the inhibitor action was experimentally observed upon replacement of the Trp86 residue,[21] which is located deeply inside the gorge. As regards the observed dramatic effect exerted by Trp86 mutation on the AChE inhibition by propidium, there is still an unresolved issue regarding the "cross-talk" between the catalytic and the peripheral sites of AChE.[42] Studies carried out by the Shafferman group led to the hypothesis of an allosteric interaction between PAS residues and Trp86,[21,42] recently confirmed in a direct experiment based on the analysis of the quenching of the fluorescence of thioflavin T bound to the PAS.[43] Insights to the molecular determinants of such an allosteric conformational effect came from the 5 ns MD simulation study performed by McCammon's group on the complex between fasciculin (Fas2) and mAChE.[41] In particular, analysis of the MD trajectories revealed that in the Fas2-bound mAChE, but not in the Fas2-unbound mAChE, the key His447 residue changed the side chain conformation in such a way as to disrupt the proton-transfer relays of the catalytic triad. We could not observe any similar effect upon binding of propidium to the PAS, confirming previous experimental evidence of such a lack of allosteric effect for small-molecule PAS ligands such as propidium and gallamine.[43,44] In relation to this, it can be observed that the PAS interaction of a small-molecule ligand like propidium seems quite different from that of Fas2, a 61-residue peptide strongly binding at an external site of AChE comprising the PAS.[19] Notably, the binding affinity constants of propidium and Fas2 to AChE are equal to 1000 and 0.0023 nM,[40] respectively. In the MD simulations of the Fas2/mAChE complex, McCammon and co-workers found that the two proteins kept their close binding during the simulation time.[41] As a matter of fact, these authors counted as much as 83 buried polar contact pairs at the interface between the two molecules. However, it is noted that Met33 plays a crucial role in the binding of Fas2 at the surface of AChE because it was shown to establish a hydrophobic interaction with Trp286.[26] In our case, the number of ligand/protein contacts is much lower, and moreover, the ligand−solvent interactions might become strongly competitive especially in the case of polar ones.

Perspectives in Drug Design. The binding of propidium to the PAS causes an inhibition of the catalytic activity of AChE that was kinetically ascribed to a mere "steric blockade" mechanism.[43,44] This hypothesis rules out the possibility of an allosteric effect arising from the cross-talk between catalytic and peripheral sites and seems to be confirmed by the crystallographic analysis[20] and by our MD simulations as well. In such a context, propidium and eventually other small-molecule PAS ligands would exert a dual biological action by inhibiting both the catalytic and the noncatalytic functions of AChE. With regard to the latter, it would be of high interest to study the possibility of blocking the proaggregatory activity of AChE toward Aβ. In fact, the central role of this substance in the neurotoxic cascade associated with Alzheimer's syndrome is well-known,[10] and growing evidence highlights the ability of AChE to induce the fibrillization of Aβ.[7,8] Actually, De Ferrari et al. have recently identified the structural determinants of the interaction between AChE and Aβ.[12] In particular, these authors carried out docking simulations between the crystal structure of *Torpedo californica* (Tc) AChE and Aβ along with kinetic studies. In this way, they found four putative binding sites of Aβ onto Tc AChE, one of which contains PAS residues. Arg289, Ser286, and Trp279 are indicated among others as Tc AChE residues responsible for the interaction with the Aβ peptide. Interestingly, these amino acids correspond to Arg296, Ser293, and Trp286 of the HuAChE, and in the present study, they were identified as residues clearly involved in the interaction between propidium and HuAChE. One might thus hypothesize that propidium is able to displace Aβ from its binding site at the HuAChE PAS, thus preventing the chaperon-like action of HuAChE toward the Aβ fibrillization. In this respect, this study can shed light on the inhibitory activity of propidium toward this intriguing noncatalytic action of HuAChE and provide a working model for the rational design of new molecules endowed with a favorable profile to treat AD patients. The combined docking and MD simulations approach presented here might be useful in the design of molecules showing an affinity toward the HuAChE PAS.

Conclusions

In this paper, we presented a combined study in which docking and MD simulations were employed in order to provide an explanation of the molecular mechanism of HuAChE inhibition carried out by the small-molecule peripheral site ligand propidium. After a flexible docking protocol, 2.5 ns MD simulations were carried out on six propidium/HuAChE complexes to identify the PAS amino acids dynamically involved in the binding. The ligand−enzyme interaction models, chosen on the basis of both docking energy score and dynamic stability of the complexes throughout the MD simulations, were similar to those experimentally determined with the murine enzyme. This suggests the possibility of employing the present modeling strategy for the definition of binding modes of small molecules to surface-like binding sites and for the exploration of ligand/target systems of pharmacological interest in the search of new selective molecules able to interfere with disease-related biochemical pathways.

Acknowledgment. This work was supported by grants from the University of Bologna (funds for selected research topics).

Supporting Information Available: Docking models and snapshots from MD simulations as PDB files. This

material is available free of charge via the Internet at http://pubs.acs.org.

References

(1) Sedo, A.; Mandys, V.; Krepela, E. Cell membrane-bound proteases: not "only" proteolysis. *Physiol. Res.* **1996**, *45*, 169−176.
(2) Charney, A. N.; Alexander-Chacko, J.; Gummaconda, R.; Egnor, R. W. Non-catalytic role of carbonic anhydrase in rat intestinal absorption. *Biochim. Biophys. Acta* **2002**, *1573*, 141−148.
(3) Tian, X.; Rusanescu, G.; Hou, W.; Schaffhausen, B.; Feig, L. A. PDK1 mediates growth factor-induced Ral-GEF activation by a kinase-independent mechanism. *EMBO J.* **2002**, *21*, 1327−1338.
(4) Kitazono, A. A.; Kron, S. J. An essential function of yeast cyclin-dependent kinase Cdc28 maintains chromosome stability. *J. Biol. Chem.* **2002**, *277*, 48627−48634.
(5) Soreq, H.; Seidman, S. Acetylcholinesterase—new roles for an old actor. *Nat. Rev. Neurosci.* **2001**, *2*, 294−302.
(6) Giacobini, E. Cholinesterase inhibitors: from the Calabar bean to Alzheimer's disease. *Cholinesterases and Cholinesterase Inhibitors*; Martin Dunitz Ltd.: London, 2000; pp 181−226.
(7) Inestrosa, N. C.; Alvarez, A.; Perez, C. A.; Moreno, R. D.; Vicente, M.; Linker, C.; Casanueva, O. I.; Soto, C.; Garrido, J. Acetylcholinesterase accelerates assembly of amyloid-beta-peptides into Alzheimer's fibrils: possible role of the peripheral site of the enzyme. *Neuron* **1996**, *16*, 881−891.
(8) Bartolini, M.; Bertucci, C.; Cavrini, V.; Andrisano, V. Beta-amyloid aggregation induced by human acetylcholinesterase: inhibition studies. *Biochem. Pharmacol.* **2003**, *65*, 407−416.
(9) Rees, T.; Hammond, P. I.; Soreq, H.; Younkin, S.; Brimijoin, S. Acetylcholinesterase promotes beta-amyloid plaques in cerebral cortex. *Neurobiol. Aging* **2003**, *24*, 777−787.
(10) Hardy, J.; Selkoe, D. J. The amyloid hypothesis of Alzheimer's disease: progress and problems on the road to therapeutics. *Science* **2002**, *297*, 353−356.
(11) Johnson, G.; Moore, S. W. The adhesion function on acetylcholinesterase is located at the peripheral anionic site. *Biochem. Biophys. Res. Commun.* **1999**, *258*, 758−762.
(12) De Ferrari, G. V.; Canales, M. A.; Shin, I.; Weiner, L. M.; Silman, I.; Inestrosa, N. C. A structural motif of acetylcholinesterase that promotes amyloid β-peptide fibril formation. *Biochemistry* **2001**, *40*, 10447−10457.
(13) Taylor, P.; Lappi, S. Interaction of fluorescence probes with acetylcholinesterase. The site and specificity of propidium binding. *Biochemistry* **1975**, *14*, 1989−1997.
(14) Radic, Z.; Reiner, E.; Taylor, P. Role of the peripheral anionic site on acetylcholinesterase: inhibition by substrates and coumarin derivatives. *Mol. Pharmacol.* **1991**, *39*, 98−104.
(15) Szegletes, T.; Mallender, W. D.; Thomas, P. J.; Rosenberry, T. L. Substrate binding to the peripheral site of acetylcholinesterase initiates enzymatic catalysis. Substrate inhibition arises as a secondary effect. *Biochemistry* **1999**, *38*, 122−133.
(16) Mallender, W. D.; Szegletes, T.; Rosenberry, T. L. Acetylthiocholine binds to asp74 at the peripheral site of human acetylcholinesterase as the first step in the catalytic pathway. *Biochemistry* **2000**, *39*, 7753−7763.
(17) Day, T.; Greenfield, S. A. A non-cholinergic, trophic action of acetylcholinesterase on hippocampal neurones in vitro: molecular mechanisms. *Neuroscience* **2002**, *111*, 649−656.
(18) Harel, M.; Schalk, I.; Ehret-Sabatier, L.; Bouet, F.; Goeldner, M.; Hirth, C.; Axelsen, P. H.; Silman, I.; Sussman, J. L. Quaternary ligand binding to aromatic residues in the active-site gorge of acetylcholinesterase. *Proc. Natl. Acad. Sci. U.S.A.* **1993**, *90*, 9031−9035.
(19) Harel, M.; Kleywegt, G. J.; Ravelli, R. B.; Silman, I.; Sussman, J. L. Crystal structure of an acetylcholinesterase−fasciculin complex: interaction of a three-fingered toxin from snake venom with its target. *Structure* **1995**, *3*, 1355−1366.
(20) Bourne, Y.; Taylor, P.; Radic, Z.; Marchot, P. Structural insights into ligand interactions at the acetylcholinesterase peripheral anionic site. *EMBO J.* **2003**, *22*, 1−12.
(21) Barak, D.; Kronman, C.; Ordentlich, A.; Ariel, N.; Bromberg, A.; Marcus, D.; Lazar, A.; Velan, B.; Shafferman, A. Acetylcholinesterase peripheral anionic site degeneracy conferred by amino acid arrays sharing a common core. *J. Biol. Chem.* **1994**, *269*, 6296−6305.
(22) Halperin, I.; Ma, B.; Wolfson, H.; Nussinov, R. Principles of docking: An overview of search algorithms and a guide to scoring functions. *Proteins* **2002**, *47*, 409−443.
(23) Karplus, M.; McCammon, J. A. Molecular dynamics simulations of biomolecules. *Nat. Struct. Biol.* **2002**, *9*, 646−652.
(24) Kua, J.; Zhang, Y.; McCammon, J. A. Studying enzyme binding specificity in acetylcholinesterase using a combined molecular dynamics and multiple docking approach. *J. Am. Chem. Soc.* **2002**, *124*, 8260−8267.
(25) Huse, M.; Kuriyan, J. The conformational plasticity of protein kinases. *Cell* **2002**, *109*, 275−282.
(26) Kryger, G.; Harel, M.; Giles, K.; Toker, L.; Velan, B.; Lazar, A.; Kronman, C.; Barak, D.; Ariel, N.; Shafferman, A.; Silman, I.; Sussman, J. L. Structures of recombinant native and E202Q mutant human acetylcholinesterase complexed with the snake-venom toxin fasciculin-II. *Acta Crystallogr., Sect. D: Biol. Crystallogr.* **2000**, *56* (11), 1385−1394.
(27) Cornell, W. D.; Cieplak, P.; Bayly, C. I.; Gould, I. R.; Merz, K. M.; Ferguson, D. M.; Spellmeyer, D. C.; Fox, T.; Caldwell, J. W.; Kollman, P. A. A second generation force field for the simulation of proteins, nucleic acids, and organic molecules. *J. Am. Chem. Soc.* **1995**, *117*, 5179−5197.
(28) Subramanian, E.; Trotter, J.; Bugg, C. E. Crystal structure of ethidium bromide. *J. Cryst. Mol. Struct.* **1971**, *1*, 3−15.
(29) Stewart, J. P. P. Optimization of parameters for semiempirical methods I. Method. *J. Comput. Chem.* **1989**, *10*, 209−220.
(30) Bayly, C. I.; Cieplak, P.; Cornell, W. D.; Kollman, P. A. A well-behaved electrostatic potential based method using charge restraints for determining atom-centered charges: the RESP model. *J. Phys. Chem.* **1993**, *97*, 10269−10280.
(31) Kuntz, I. D.; Blaney, J. M.; Oatley, S. J.; Langridge, R.; Ferrin, T. E. A geometric approach to macromolecule−ligand interactions. *J. Mol. Biol.* **1982**, *161*, 269−288.
(32) Dougherty, D. A. Cation−π interactions in chemistry and biology: a new view of benzene, Phe, Tyr, and Trp. *Science* **1996**, *271*, 163−168.
(33) Meng, E. C.; Shoichet, B. K.; Kuntz, I. D. Automated docking with grid-based energy evaluation. *J. Comput. Chem.* **1992**, *13*, 505−524.
(34) Case, D. A.; Pearlman, D. A.; Caldwell, J. W.; Cheatham, T. E., III; Wang, J.; Ross, W. S.; Simmerling, C. L.; Darden, T. A.; Merz, K. M.; Stanton, R. V.; Cheng, A. L.; Vincent, J. J.; Crowley, M.; Tsui, V.; Radmer, R. J.; Duan, Y.; Pitera, J.; Massova, I.; Seibel, G. L.; Singh, U. C.; Weiner, P. K.; Kollman, P. A. *AMBER 7*; University of California: San Francisco, 2002.
(35) Jorgensen, W. L.; Chandrasekhar, J.; Madura, J. D.; Impey, R. W.; Klein, L. M. Comparison of simple potential functions for simulating liquid water. *J. Chem. Phys.* **1983**, *79*, 926−935.
(36) Berendsen, H. J. C.; Postma, J. P. M.; Van Gunsteren, W. F.; Di Nola, A.; Haak, J. R. Molecular dynamics with coupling to an external bath. *J. Chem. Phys.* **1984**, *81*, 3684−3690.
(37) Essmann, U.; Perera, L.; Berkowitz, M. L.; Darden, T.; Lee, H.; Pedersen, L. G. A smooth particle mesh Ewald method. *J. Chem. Phys.* **1995**, *103*, 8577−8593.
(38) Ryckaert, J. P.; Ciccotti, G.; Berendsen, H. J. C. Numerical integration of the Cartesian equations of motion of a system with constraints: molecular dynamics of *n*-alkanes. *J. Comput. Phys.* **1977**, *23*, 327−341.
(39) *ClogP*, version 4.3; BioByte Corp.: Claremont, CA, 2002.
(40) Reiner, E.; Radic, Z. Mechanism of action of cholinesterase inhibitors. *Cholinesterases and Cholinesterase Inhibitors*; Martin Dunitz Ltd.: London, 2000; pp 103−119.
(41) Tai, K.; Shen, T.; Henchman, R. H.; Bourne, Y.; Marchot, P.; McCammon, J. A. Mechanism of acetylcholinesterase inhibition by fasciculin: a 5-ns molecular dynamics simulation. *J. Am. Chem. Soc.* **2002**, *124*, 6153−6161.
(42) Ordentlich, A.; Barak, D.; Kronman, C.; Flashner, Y.; Leitner, M.; Segall, Y.; Ariel, N.; Cohen, S.; Velan, B.; Shafferman, A. Dissection of the human acetylcholinesterase active center determinants of substrate specificity. Identification of residues constituting the anionic site, the hydrophobic site, and the acyl pocket. *J. Biol. Chem.* **1993**, *268*, 17083−17095.
(43) De Ferrari, G. V.; Mallender, W. D.; Inestrosa, N. C.; Rosenberry, T. L. Thioflavin T is a fluorescent probe of the acetylcholinesterase peripheral site that reveals conformational interactions between the peripheral and acylation sites. *J. Biol. Chem.* **2001**, *276*, 23282−23287.
(44) Szegletes, T.; Mallender, W. D.; Rosenberry, T. L. Nonequilibrium analysis alters the mechanistic interpretation of inhibition of acetylcholinesterase by peripheral site ligands. *Biochemistry* **1998**, *37*, 4206−4216.

JM040787U